



LAWRENCE
LIVERMORE
NATIONAL
LABORATORY

Developing Large-Scale Forcing Data for Single-Column Model and Cloud-Resolving Model from the Mixed-Phase Arctic Cloud Experiment

S. Xie, S. Klein, M. Zhang, J. Yio, R. Cederwall,
R. McCoy

October 20, 2005

Journal of Geophysical Research

Disclaimer

This document was prepared as an account of work sponsored by an agency of the United States government. Neither the United States government nor Lawrence Livermore National Security, LLC, nor any of their employees makes any warranty, expressed or implied, or assumes any legal liability or responsibility for the accuracy, completeness, or usefulness of any information, apparatus, product, or process disclosed, or represents that its use would not infringe privately owned rights. Reference herein to any specific commercial product, process, or service by trade name, trademark, manufacturer, or otherwise does not necessarily constitute or imply its endorsement, recommendation, or favoring by the United States government or Lawrence Livermore National Security, LLC. The views and opinions of authors expressed herein do not necessarily state or reflect those of the United States government or Lawrence Livermore National Security, LLC, and shall not be used for advertising or product endorsement purposes.

UCRL-JRNL-216375

**Developing Large-Scale Forcing Data for Single-Column and Cloud-Resolving
Models from the Mixed-Phase Arctic Cloud Experiment**

*Shaocheng Xie¹, Stephen A. Klein¹, Minghua Zhang², John J. Yio¹, Richard T. Cederwall¹, and
Renata McCoy¹*

¹Lawrence Livermore National Laboratory, Livermore, California, USA

²Marine Sciences Research Center, State University of New York, Stony Brook, New York,
USA

Submitted to: Journal of Geophysical Research

Submission Date: December 3, 2005

Manuscript No: 2005JD006950

Revised: May 3, 2006

ABSTRACT

This study represents an effort to develop Single-Column Model (SCM) and Cloud-Resolving Model (CRM) large-scale forcing data from a sounding array in the high latitudes. An objective variational analysis approach is used to process data collected from the Atmospheric Radiation Measurement program (ARM) Mixed-Phase Arctic Cloud Experiment (M-PACE), which was conducted over the North Slope of Alaska in October 2004. In this method, the observed surface and top of atmosphere measurements are used as constraints to adjust the sounding data from M-PACE in order to conserve column-integrated mass, heat, moisture, and momentum. Several important technical and scientific issues related to the data analysis are discussed.

It is shown that the analyzed data reasonably describe the dynamic and thermodynamic features of the Arctic cloud systems observed during M-PACE. Uncertainties in the analyzed forcing fields are roughly estimated by examining the sensitivity of those fields to uncertainties in the upper-air data and surface constraints that are used in the analysis. Impacts of the uncertainties in the analyzed forcing data on SCM simulations are discussed. Results from the SCM tests indicate that the bulk features of the observed Arctic cloud systems can be captured qualitatively well using the forcing data derived in this study and major model errors can be detected despite the uncertainties that exist in the forcing data as illustrated by the sensitivity tests. Finally, the possibility of using the European Center for Medium-Range Weather Forecasts (ECMWF) analysis data to derive the large-scale forcing over the Arctic region is explored.

1. Introduction

The Single-Column Model (SCM) and Cloud-Resolving Model (CRM) are two useful modeling tools in the evaluation and development of physical parameterizations used in climate models [Randall *et al.*, 1996]. This kind of modeling study has been largely scarce for the high latitudes, owing to the lack of appropriate large-scale forcing data, i.e., the vertical velocity and horizontal advective tendencies of atmospheric state variables, which are required to drive SCMs and CRMs. The forcing data used in a few available SCM/CRM studies in the Arctic regions [e.g., Pinto *et al.*, 1999; Jiang *et al.* 2000] are usually from output of operational numerical weather prediction (NWP) models because there were no suitable sounding arrays that could be used to derive the required observed forcing data. Zhang *et al.* [2001] showed that the horizontal winds from NWP models are generally more homogeneous than those from sounding data, which could result in a much weaker wind divergence than that from observations. It is also known that the NWP model-derived forcing data are largely affected by the deficiencies of the model physical parameterizations used in generating the data. As demonstrated by Xie *et al.* [2003] and Morrison and Pinto [2004], the forcing data directly obtained from the NWP model contain large errors. In order to reduce errors in the NWP model-derived forcing data, several correction algorithms were recently developed by using available observations to constrain the NWP data [e.g., Xie *et al.*, 2004; Morrison and Pinto, 2004]. The constrained NWP forcing data are useful especially for statistical studies of SCM/CRM simulations, but they are clearly less accurate than those derived from a well-defined sounding array [Xie *et al.*, 2004].

As an attempt to improve the representation of Arctic clouds and their interaction with radiation in present climate models, the U. S. Department of Energy (DOE) Atmospheric Radiation Measurement program (ARM) launched its Mixed-Phase Arctic Cloud Experiment (M-PACE) field campaign over the North Slope of Alaska (NSA) in October 2004 [Harrington and Verlinde, 2004; Verlinde *et al.*, 2005]. During the field campaign, detailed information about Arctic clouds and cloud microphysical properties were measured using the ARM Millimeter Wavelength Cloud Radar (MMCR), Micropulse Lidar (MPL), Laser Ceilometers, and three instrumented aircraft. A sounding array with four radiosonde stations (the Barrow, Atkasuk, Oliktok Point, and Toolik Lake sites represented by the large star symbols in Figure 1) was used to provide six hourly sounding measurements for most of the M-PACE period and

therefore allow for calculation of the large-scale SCM/CRM forcing data. Basic surface meteorology variables and surface radiative fluxes were available at two ARM ground base sites at Barrow and Atkasuk and at the Pacific Northwest National Laboratory (PNNL) Atmospheric Remote Sensing Laboratory (PARSL) ARM-like remote sensing facility at Oliktok Point. The National Aeronautics and Space Administration (NASA) Terra and the National Oceanic and Atmospheric Administration (NOAA) -15 and -16 satellites provided satellite measurements of broadband radiative fluxes at the top of the atmosphere (TOA).

The M-PACE field campaign provides the first chance to derive the SCM/CRM forcing data from a sounding network in the Arctic region. For this purpose, the constrained variational analysis approach developed by *Zhang and Lin* [1997] is used in this study. This method has been successfully used in processing ARM data collected at its mid-latitude Southern Great Plains (SGP) site [*Zhang et al.*, 2001]. The basic idea of the analysis approach is to use domain-averaged surface and TOA observations as the constraints to adjust the balloon soundings in order to satisfy the conservation of column integrals of mass, heat, moisture, and momentum. The resulting analyzed data are dynamically and thermodynamically consistent.

It should be noted that the data density over the NSA region is still much lower than that in other ARM field campaigns conducted at its SGP site despite the great effort made by M-PACE. For example, balloon soundings were only available 4 times per day over 4 sounding stations in M-PACE while they were available 8 times per day over a well-defined sounding network of 5 stations during the ARM SGP Intensive Operation Periods (IOPs). In addition, there were hourly horizontal wind data from seven wind profiler stations within the SGP domain to supplement the sounding measurements (see Figure 4 in *Zhang et al.* 2001). This indicates that the background field used in the variational analysis could play a more important role in the analysis of M-PACE data due to the low data density. Note that a background field is needed in the analysis for filling missing soundings and interpolating data onto the analysis grid points that do not overlap with the sounding stations. Surface data were rather sparse and were only available at three stations in M-PACE. Moreover, some of the surface fields required by the variational analysis were either not available (e.g., sensible and latent heat fluxes) or not accurately measured (e.g., surface precipitation), as discussed later. This suggests potentially large uncertainties in the domain-averaged surface constraints that are used in the variational analysis. It should be noted that the M-PACE observational network was designed on a

challenging location along the North Alaskan coast. The low cloud systems that affected the NSA site were often advected from nearby oceans during the experiment period. Thus, it might be difficult for the M-PACE observational network to fully capture the large-scale characteristics of the observed Arctic clouds.

In this study, we try to alleviate these difficulties by carefully dealing with all the technical details in the data analysis. In particular, we attempt to address the following important technical and scientific issues associated with the analysis: 1) Can the required domain-averaged constraints be reasonably derived from surface data collected at only three ground stations? 2) How sensitive are the analyzed forcing data to uncertainties in the upper-air sounding data and surface constraints? 3) What is the impact of those uncertainties in the analyzed forcing fields on SCM simulations? 4) Can physically important model errors be detected despite uncertainties in the forcing data? Moreover, given the difficulties to obtain data from a sounding array in the Arctic, it is important to investigate how to use NWP analysis data to derive useful large-scale forcing for SCM/CRM studies. This issue is also discussed in the study. A thorough discussion of the above issues will not only help SCM/CRM modelers to better use the analyzed data but also provide useful information for planning future field experiments.

The technical details of the objective analysis of M-PACE observations are described in Section 2. Basic features of the large-scale dynamic and thermodynamic structures associated with the Arctic clouds observed during M-PACE are discussed in Section 3. Section 4 shows results from the sensitivity tests, which are conducted to help understand the uncertainty of the derived forcing data due to uncertainties in the upper-air input data and surface constraints. The impact of the uncertainties in the forcing data on SCM simulations is discussed in Section 5. The possibility of using the European Center for Medium-Range Weather Forecasts (ECMWF) analysis data with the M-PACE constraints to derive the large-scale forcing is explored in Section 6. Section 7 gives summary and discussions.

2. Analysis of M-PACE observations

The constrained variational objective analysis approach developed by *Zhang and Lin* [1997] is used for the objective analysis of the data collected during M-PACE, which started on 00Z 5 October and ended on 12Z 22 October 2004 at the ARM NSA site. The technical details of this approach and its implementation for processing the data collected at the ARM SGP site

have been described in the work of *Zhang and Lin* [1997] and *Zhang et al.* [2001]. In this section, we first briefly review the approach and then discuss the details of how it is applied to analyze the M-PACE data.

2.1 The constrained variational analysis approach

The constrained variational analysis of *Zhang and Lin* [1997] was designed for deriving large-scale vertical velocity and advective tendencies from sounding measurements over a network with a small number of stations. This method uses the domain-averaged surface and TOA observations as constraints to adjust atmospheric state variables from soundings by the smallest possible amount to conserve column-integrated mass, moisture, static energy, and momentum so that the final analysis data set is dynamically and thermodynamically consistent. The column constraints can be obtained by vertically integrating the governing equations of the large-scale atmospheric fields:

$$\langle \nabla \cdot \vec{v} \rangle = -\frac{1}{g} \frac{dp_s}{dt} \quad (1)$$

$$\frac{\partial \langle q \rangle}{\partial t} + \langle \nabla \cdot \vec{v} q \rangle = E_s - P_{rec} - \frac{\partial \langle q_l \rangle}{\partial t} \quad (2)$$

$$\frac{\partial \langle s \rangle}{\partial t} + \langle \nabla \cdot \vec{v} s \rangle = R_{TOA} - R_{SRF} + LP_{rec} + SH + L \frac{\partial \langle q_l \rangle}{\partial t} \quad (3)$$

$$\frac{\partial \langle \vec{V} \rangle}{\partial t} + \langle \nabla \cdot \vec{V} \vec{V} \rangle + f \vec{k} \times \langle \vec{V} \rangle + \nabla \langle \phi \rangle = \vec{\tau}_s \quad (4)$$

where

$$\langle X \rangle = \frac{1}{g} \int_{p_t}^{p_s} (X) dp$$

In the above, \vec{v} is the wind, $s = C_p T + gz$ is the dry static energy, C_p is heat capacity at constant pressure for dry air, g is gravitational acceleration, q is the mixing ratio of water vapor, q_l is the cloud liquid and ice water content, R is the net downward radiative flux at TOA and at the surface (SRF), τ_s is the surface wind stress, P_{rec} is precipitation, L is the latent heat of vaporization, SH is the sensible heat flux, E_s is the surface evaporation, f is Coriolis parameter, ϕ is geopotential height, \vec{k} is unit vector in the vertical direction, p_s is the surface pressure, and p_t is the TOA pressure.

The final analysis product is derived by minimizing the cost function:

$$I(t) = \iiint_{p,x,y} [\alpha_u (u^* - u_0)^2 + \alpha_v (v^* - v_0)^2 + \alpha_s (s^* - s_0)^2 + \alpha_q (q^* - q_0)^2] dx dy dp \quad (5)$$

with (1) – (4) as strong constraints, where superscript “*” denotes final analysis and subscript “o” denotes initial analysis. α is the weighting function related to error estimates in the initial input. In this study, we use the objective analysis scheme described in *Cressman* [1959] to obtain the initial analysis field from the M-PACE sounding array. The *Cressman* scheme requires a background field for filling missing soundings and interpolating data onto the analysis grids that do not overlap with the sounding stations. The rationales of our analysis strategy and implementation details of the variational analysis to process M-PACE data are discussed below.

2.2 Implementation details of the variational analysis to M-PACE observations

Figure 1 displays the objective analysis domain and analysis grid points (A1-A6, solid circles) defined for analyzing the M-PACE data. It is seen that the analysis domain is different from the M-PACE sounding network. In our analysis, the Toolik Lake site is not used as one of the analysis grid points because this station rests on a much higher location (760 m) than the other three sounding stations (less than 30 m), and using this site could cause problems in obtaining the domain-averaged quantities required by the variational analysis. Note that it is not necessary (although it is common) to use ground sounding stations as the analysis grid points in an objective analysis because sounding balloons can drift away from their ground stations anyway while ascending. In the defined domain, the analysis grid points A1, A2, and A5 overlap with the sounding stations at the Barrow, Atqasuk, and Oliktok Point sites, respectively. In order to still make use of the sounding information collected from the Toolik Lake site, we define an extra analysis point (A4) with the surface elevation of 50 m as shown in Figure 1. Following *Zhang et al.* [2001], we also add another two auxiliary grid points at the middle of the two long sides of the domain (i.e., A3 and A6 in Figure 1) to improve the linear assumption, which is used in the variational analysis to derive the fluxes into or out of the analysis domain. The grid points A1-A6 consist of the final objective analysis grid points used in this study and the final analyzed fields represent an average over the domain encompassed by these analysis

grid points, which is about 230 km in the longitudinal direction and 100 km in the latitudinal direction.

M-PACE conducted two radiosonde Intensive Operational Periods (IOPs) to measure the vertical profiles of temperature, relative humidity, and horizontal winds every six hours at the four ARM sounding stations. The first radiosonde IOP was from 00Z 5 October to 00Z 10 October 2004 and the second one from 00Z 14 October to 12Z 22 October 2004. Between the two IOPs, sounding data were available once a day at the Barrow and Atkasuk sites. To complement the ARM observations, the 12-hourly soundings at the National Weather Service (NWS) Barrow station are also used in the analysis in order to maximize the use of the limited observations available in the Arctic regions. Similar to *Zhang et al.* [2001], these measured upper-air data are first analyzed using the analysis scheme of *Cressman* [1959] but with background fields from 0.5 x 0.5 degree ECMWF analysis data, whose grid points are shown by the “plus” symbols in Figure 1.

As discussed earlier, the accuracy of the background data could play a more important role in the objective analysis of M-PACE data due to the low data density in the NSA region. For the M-PACE period, we have archived NWP model analysis data from both ECMWF and NCEP (the U. S. National Center for Environmental Prediction). The NWP models used to generate the analysis data are the ECMWF T511L60 (~ 40km) model [*ECMWF*, 2004] and the NCEP ETA-12 (12 km and 60 Levels) mesoscale model [*Rogers et al.*, 2001] (courtesy of Dr. Anton Beljaars of ECMWF and Dr. Eric Rogers of NCEP). The 12-hourly soundings at the NWS Barrow station were assimilated into both the ECMWF and NCEP data analysis system. An initial investigation indicates that the ECMWF analysis has smaller errors than the NCEP ETA analysis over the ARM NSA site in comparison with the M-PACE data. Figures 2a-d give the root-mean square (RMS) error of the ECMWF analysis and the ETA analysis from the M-PACE sounding observations over the Barrow station for horizontal winds, temperature, and relative humidity, respectively. Similar results are seen at the other sounding stations. For the M-PACE period, both analyses typically represent well the temporal evolutions of these fields (not shown). The RMS error of the ECMWF analysis is typically less than 1.5 m s⁻¹ in horizontal winds, 1 K in temperature, and 13% in relative humidity. The ETA analysis shows much larger errors in the horizontal winds than the ECMWF analysis. The errors in the temperature and relative humidity are comparable for these two model analysis datasets. As

shown in *Xie et al.* [2006a], the errors in the ECMWF analysis are partially related to the errors in its simulated cloud systems during M-PACE. However, it is not clear why the ETA analysis has much larger errors in the horizontal winds than the ECMWF analysis. This could be a subject of future study.

The required column constraints can be obtained from measurements at the two ARM ground-based sites at Barrow and Atqasuk and the PARSL remote sensing facility at Oliktok Point (Figure 1). The ARM surface instruments and the PARSL ARM-like remote sensing facility provided measurements of surface precipitation, pressure, horizontal winds, temperature, relative humidity, surface broadband upwelling and downwelling radiative fluxes, column precipitable water, and cloud liquid water path. The radiative fluxes at TOA are from the 1 x 1 degree analysis of the NASA Terra and the NOAA-15 and NOAA-16 satellite data. The algorithm used to create the TOA radiative fluxes is described in *Minnis et al.* [2001]. It should be noted that the ARM observed precipitation could be overestimated due to blowing snow. In the analysis, we merged the ARM-observed surface precipitation data with those measured at the National Weather Service (NWS) Barrow station. The ARM precipitation record is multiplied by a constant, which is equal to the ratio of a “weighted” average of the ARM time mean precipitation and NWS time mean precipitation to the average precipitation from the ARM data for the M-PACE. This scale factor is computed at Barrow and applied to other stations. In the current analysis, more weights (0.75) were given to the NWS data, which were thought to be more reliable and more consistent with the information recorded in the experiment synoptic logs during M-PACE (Dr. James Pinto, University of Colorado, personal communication). It should be noted that the observed surface precipitation contained rather large uncertainty even with the correction based on the NWS data, which could experience the same problems with blowing snow as the ARM observations. In section 4, we conduct a sensitivity test to demonstrate how this impacts analyzed forcing fields.

Since the observed surface sensible and latent heat required by the variational analysis are not available, these fields are currently calculated by:

$$HFLX = f_{ind} * HFLX_{bulk_land} + (1-f_{ind}) * HFLX_{EC_ocean} \quad (6)$$

where $HFLX$ represents surface sensible heat flux (SH) or latent heat flux (LH). f_{land} is the land fraction of the analysis domain. $HFLX_{bulk_land}$ represents the heat fluxes over land. They are calculated using the bulk flux algorithm described by *Fairall et al.* [1996] with some modifications so that it can be suitable for use over a surface covered by snow or ice, which is the case for M-PACE. All the required inputs for the bulk flux algorithm, such as surface temperature, moisture, horizontal winds, and pressure, are from M-PACE observations. The details of the implementation of the bulk flux algorithm to M-PACE data were described in *Xie et al.* [2006a]. $HFLX_{EC_ocean}$ denotes the ECMWF model-produced ocean heat fluxes. We include the heat fluxes over ocean in order to partially retain the important influence of the surface fluxes over open ocean on the observed boundary-layer clouds, which were formed over the open ocean to the northeast of the Alaskan coast and then advected over the NSA site.

To obtain the domain-averaged quantities for other fields, we first interpolate the observations at the three ARM ground-base stations (A1, A2, and A5) onto the three extra analysis grid points (A3, A4, and A6) using an interpolation scheme described in *Barnes* [1964]. The weighting function in the Barnes scheme is dependent on the distance between an analysis grid point and the measurement stations. This could help reduce the derived domain-average quantities overweighted by data measured at Barrow and Atqasuk along the west boundary of the domain. A simple arithmetic averaging was then used to obtain the domain-averaged quantities.

Can measurements at the three stations represent well the temporal and spatial variations of these surface fields over the entire domain? Given the data availability at the NSA, it is impossible to study this issue from observations. In this study, we use the 0.5 x 0.5 degree ECMWF model output data to help understand the problem and roughly estimate uncertainties that could be introduced in the domain-averaged fields due to the low density of surface data. For this purpose, we constructed domain-averaged quantities from the model data in two different ways. One set of the domain-averaged quantities was obtained by just averaging data at the three model land grid points nearest to Barrow, Atqasuk, and Oliktok Point, and the other one was obtained by averaging all model land grid points within the analysis domain.

Figures 3a-d compare the domain-averaged results constructed by these two methods for surface precipitation, net surface radiation, sensible heat flux, and latent heat flux, respectively. In the figure, we use AVG3PTS and AVGALL to represent the two model-constructed datasets, respectively. Note that negative values in sensible and latent heat fluxes represent heat transport

from atmosphere to surface. It is seen that the temporal variability of these two datasets is in excellent agreement with correlation coefficient over 0.95 for precipitation, 0.97 for sensible heat flux, 0.99 for latent heat flux, and 0.99 for net surface radiation. For the magnitude of these fields, however, noticeable differences are seen in surface precipitation, sensible heat flux, and latent heat flux, indicating a quite large spatial variability of these fields. The time-mean values over the entire M-PACE period for these two datasets (the numbers behind legend labels in the Figures 3a-d) suggest that averaging over only the three stations might underestimate precipitation by about 20% and overestimate sensible and latent heat fluxes by about 20% and 40%, respectively. It is interesting to see that the two constructed datasets have a good agreement in the magnitude of surface net radiation, in which AGV3PTS only slightly overestimates AVGALL by about 6%.

It should be noted that the differences shown in these two constructed datasets are solely based on the ECMWF model forecasts and may not fully reflect those in the real world because the model does not have the true world's small-scale variability. Figure 3 only provides some useful information for us to roughly estimate potential errors in the domain-averaged fields resulting from the lack of dense surface observations over the NSA region. The above discussions indicate that the errors in the domain-mean quantities introduced by using only three stations are not likely to affect the temporal evolution of analyzed forcing fields but may have impacts on the magnitude. They also suggest the need to have a denser surface observation network in order to improve the quality of the domain-averaged quantities, which are not only used as the constraints in the variational analysis but also used as the observational data to evaluate model performance.

3. Analyzed fields

Figures 4a-d show the time-pressure cross sections of analyzed horizontal winds, temperature, and water vapor mixing ratio, respectively. For the period 5 to 13 October, the upper-air circulations were typically characterized by the west-northwesterly flow in the middle and upper troposphere and the east-northeasterly flow in the lower troposphere and near the surface, associated with an upper level cold trough and a strong surface high-pressure system centered to the northeast of the Alaskan coast. There was a substantial temperature decrease below 665 hPa and a sharp moisture decrease for the period 8-13 October over the NSA site. The

ARM ARSCL (the Active Remotely-Sensed Clouds Locations, *Clothiaux et al.* 2000) data indicated the appearance of multilayered clouds in the mid- and low-levels during the period 6-7 October and persistent mixed-phase boundary layer clouds during the period 8-14 October as shown in Figure 5a. Frequent light snow events were reported in the ARM and NWS ground measurements during this period (Figure 5b).

After 14 October, the mixed-phase boundary layer clouds started to disappear as a warm front moved through the area on 15-16 October and a deep ridge moved over the NSA. The analyzed wind fields show that southwesterly flow prevailed in the entire troposphere except on late 19 October when there was an abrupt wind direction change from the southwest to the southeast associated with a strong warm frontal passage. The upper-air started to warm-up and become moist when the warm ridge was moving into the NSA. The significant temperature and moisture increase on 19 October was the result of the strong warm front approaching the NSA site. This period is dry and no snow was reported except on late 19 October when the strong frontal system moved into the NSA from the southwest bringing deep prefrontal and frontal clouds and producing large snowfall (Figures 5a-b).

The large-scale vertical velocity (ω) derived from the M-PACE observations using the variational analysis approach is shown in Figure 6a. Since the tropopause in the Arctic is usually lower than 215 hPa, the TOA is set to 215 hPa in the variational analysis and ω is set to zero above this level. The analyzed vertical velocity field generally shows strong downward motion above cloud top and relatively weak upward motion at low levels for the period 6-14 October where multilayered clouds and boundary layer clouds occurred. The downward motion is much stronger for the period 8-14 October when only low-level clouds appeared compared to the earlier period. The strong downward motion limits the vertical extension of clouds and confines clouds in the low levels. After 14 October, episodes of strong downward motion and weak upward motion are shown in the analyzed ω field. The strong upward motion on late 19 October is associated with the strong frontal passage mentioned earlier and consistent with the large front-produced snow as seen in Figure 5b.

Figure 6b shows analyzed total advective tendencies of temperature, which includes the adiabatic expansion term. The temperature tendency field is closely associated with the ω field. In general, large-scale warming (cooling) corresponds to downward (upward) motion. From 5 October to 12 October, Figure 6b generally shows warm advective tendency in the

middle troposphere associated with the strong downward motion and cold advective tendency in the lower troposphere due to both upward motion and horizontal cold advection (not shown). In the case of the strong frontal passage on late 19 October, there is a strong advective cooling associated with the strong upward motion. This is a typical dynamic and thermodynamic structure of a frontal cloud system.

The moisture advection field shown in Figure 6c indicates a quite strong moisture convergence between 965 hPa and 515 hPa on 5 October prior to the formation of the multi-layer clouds. A moisture divergence is seen during the period 8–12 October, which is consistent with the moisture decrease shown in Figure 4d. This also suggests the observed boundary layer clouds were most likely advected into the ARM NSA site from the open ocean rather than being formed locally. For the period 13–17 October, we see a moisture convergence in the analyzed field, which leads to the recovery of water vapor as shown in Figure 4d. There is strong moisture convergence during the strong frontal passage on late 19 October, corresponding to the strong upward motion, cold advection, and large surface precipitation as discussed earlier.

The consistency between the large-scale forcing and the observed cloud systems indicates that the large-scale dynamical fields are derived qualitatively well from the M-PACE observations. In Figures 7 and 8 we further examine the components of column-integrated heat and moisture budgets, respectively. For the period 5–12 October, the column radiative cooling is the dominant term in the heat budgets (Figure 7). This term is offset mainly by the latent heating associated with surface precipitation. The overall effect leads to a slight heat loss shown in the local heat storage term. After 12 October, the horizontal heat convergence becomes the dominant term to offset the radiative cooling, leading to an increase of local heat storage until the strong front passed over the NSA site on late 19 October where a large energy loss occurred in the local heat storage term. The heat loss is associated with the strong horizontal cold advection that is partially offset by the latent heat release due to condensation. The two heat convergence peaks on 15 October and early 19 October are associated with the warm fronts approaching the NSA site. The sensible heat flux is a small term compared to other budget terms in the entire M-PACE period.

In the moisture budgets (Figure 8), the two largest terms are the local moisture storage term and the horizontal moisture convergence. Precipitation is also important, especially during the period of the strong frontal passage on late 19 October, where the moisture storage term

shows a rapid moisture increase associated with a strong horizontal moisture convergence. Surface evaporation is much smaller than other terms in the moisture budgets.

4. Uncertainty in the analyzed forcing fields

In the last section we showed that the analyzed forcing fields exhibited reasonable dynamic and thermodynamic structures corresponding to the observed Arctic clouds. In this section we estimate the accuracy of the derived forcing data by examining the sensitivity of those data to potential uncertainties in the upper-air data and surface constraints used in the variational analysis. For this purpose, three sensitivity tests are conducted to illustrate the impacts of uncertainties in upper-air data, domain-averaged surface precipitation, and surface sensible and latent heat fluxes on the analyzed forcing fields, respectively. Note that these sensitivity tests are particularly necessary for field experiments conducted in the Arctic region because of the low data density there. The sensitivity tests can provide a crude estimate of the accuracy limit in the derived forcing fields. In the following discussion, the current objective analysis is considered as the control case and is represented by Exp0. Table 1 lists the sensitivity tests carried out in this study and described below.

The first sensitivity test (Exp1) is performed to examine the sensitivity of the forcing data to uncertainties in the upper air sounding data, which were obtained using a Vaisala Radiosonde RS92 balloon-borne sounding system. As reported in *Lesht* [2005], the RS92 sondes substantially reduce the well-known dry bias with Vaisala RS80 series of sondes, although they do seem to be biased dry during daytime in the upper troposphere at lower latitudes where solar effects are greatest. The instrument and measurement accuracy at NSA is of about 0.5 m s^{-1} in the horizontal winds, 0.5 K in the temperature, and 5% in the relative humidity. The uncertainty in humidity soundings could be larger when temperature is below -40C due to a slow response time of the instrument. In this test, random errors are added to horizontal wind components, temperature, and water vapor mixing ratio fields. These random errors are bounded by a RMS error of 1.5 m s^{-1} for the wind components, 0.5 K for the temperature, and 5% of the locally observed water vapor mixing ratio for the moisture. Note that larger than the reported errors are added in the horizontal winds in order to consider scale aliasing and invalid and missing measurement errors due to the insufficient samplings in the field experiment.

The second sensitivity test (Exp2) is conducted to examine how sensitive the derived forcing fields are to uncertainties in the domain-averaged surface precipitation. *Zhang et al* [2001] showed that the accuracy of the domain-averaged precipitation had the largest impact on the derived forcing fields. Unfortunately, as noted earlier, considerably large uncertainties existed in the ARM surface precipitation measurement during M-PACE because of blowing snow and the lack of dense observations. In the current analysis (Exp0), we merged the ARM-observed surface precipitation with the precipitation data measured at the NWS Barrow station with three-fourths weights given to the NWS data because the latter was thought to be more reliable. However, the choice of the weighting coefficients for the merging is rather arbitrary. In the sensitivity test, we merge the two datasets with equal weight. Figure 5b compares the surface precipitation rates used in the control analysis (Pr0) and that used in the sensitivity test (Pr1). It is seen that Pr1 is consistently larger than Pr0 since the ARM-observed precipitation is significantly larger than the NWS-observed. The difference between Pr0 and Pr1 is much larger than that caused by using different numbers of stations to obtain the domain mean as shown in Figure 3a.

The third test (Exp3) is to examine the sensitivity of the derived forcing data to uncertainties in the domain-averaged surface sensible and latent heat fluxes. In the control analysis, the surface heat fluxes are an average of the fluxes from both ocean and land regions within the analysis domain in order to better represent these fields associated with the observed boundary-layer cloud systems, which were mainly driven by large sensible and latent heat fluxes over the open ocean and advected into the NSA site. Preliminary SCM tests indicate that including the fluxes over the ocean is important for some models to correctly capture major features of the observed boundary layer clouds (Dr. Hugh Morrison, National Center for Atmospheric Research, personal communication). As discussed in Section 2, however, all other domain-averaged surface fields are derived from observations at the three land stations, i.e., Barrow, Atqasuk, and Oliktok Point. There is an inconsistency in deriving the domain-averaged quantity between surface sensible and latent heat fluxes and other variables. In Exp3, we use the surface heat fluxes over land only to examine how sensitive the derived forcing fields are to this change. Figures 9a-b compare the sensible and latent heat fluxes used in the control analysis (SH0 and LH0) and those used in Exp3 (SH1 and LH1), respectively. The largest differences are seen for the periods 5–13 October where SH0 is positive, reflecting a large heat transport

from the warm open ocean to the atmosphere. Meanwhile the sensible heat flux over land (SH1) shows negative values during this period, consistent with the observed near-surface temperature inversion over land. By including ocean grid points, LH0 is much larger than that averaged only over land (LH1). It is interesting to see that the two surface heat flux datasets agree well with each other after 14 October. Similar to Exp2, the difference in the sensible and latent heat fluxes between Exp3 and the control analysis is also much larger than that due to using only three stations (i.e., low density grid points on land only) to obtain the domain mean and thus representing a worse scenario than the uncertainties shown in Figures 3c and 3d.

Figure 10 shows the time-pressure cross section of the derived large-scale omega fields from the three sensitivity tests and their difference from the control analysis. The temporal and vertical distributions of the omega fields derived in these tests (Figures 10 a-c) are very similar to those shown in the control analysis (Figure 6a). The omega change due to the use of the perturbed upper-air input data (Exp1) is quite random (Figure 10d), consistent with the random errors added to the state variables. The random errors also lead to a higher temporal variability in the derived omega field from Exp1. The difference in the omega field between Exp1 and Exp0 is typically around 1 hPa hr^{-1} , which is about 20% of the typical vertical velocities in the control run. This suggests uncertainties in the derived forcing data resulting from errors in the upper-air sounding data cannot be neglected.

The stronger precipitation used in Exp2 results in stronger upward motion and weaker downward motion in the middle and lower troposphere during the precipitation periods in comparison with Exp0 as indicated in Figure 10e. This is because stronger precipitation needs more moisture convergence into the column and therefore stronger upward motion. The magnitude of the omega difference due to the change in the surface precipitation is up to 3 hPa hr^{-1} , which is larger than that in Exp1, in which the upper-air data are perturbed. Considering that the upward motion is quite weak in these weak precipitation events, the difference shown in Figure 10e is rather significant. This indicates the importance of an accurate measurement of surface precipitation in improving the accuracy of the analyzed forcing fields.

Compared to Exp0, the smaller sensible and latent heat fluxes used in Exp3 lead to a slightly stronger upward motion in mid- and low-levels and a slightly stronger downward motion in upper levels for the period 9-12 October, which corresponds to the largest heat flux difference between Exp3 and Exp0 as shown in Figure 9. The magnitude of the omega change is less than

1 hPa hr^{-1} . This small change in the omega field is partially due to the compensation between the change caused by sensible heat flux and that by latent heat flux. The reduction of sensible heat flux and latent heat flux in Exp3 acts in different ways to the omega field. It is seen from Eq. (3) that smaller sensible heat flux leads to stronger convergence of dry static energy and therefore stronger downward motion if other terms on the right-hand side of the equation are unchanged in order to keep the same local change rate of dry static energy. Reduction of latent heat flux plays the same role as increase of surface precipitation, resulting in more moisture convergence and therefore stronger upward motion, as indicated in Eq. (2).

5. Impacts on SCM simulations

In section 4 we discussed potential uncertainties in the derived large-scale forcing data due to errors in the upper-air data and the column constraints. One important issue is how SCMs respond to these uncertainties in the forcing data. Can a SCM driven by these forcing datasets produce similar results so that the same model deficiencies can be detected? To address these issues, the SCM version of the National Center for Atmospheric Research (NCAR) Community Atmosphere Model version 3 (SCAM3) is used in this study. *Collins et al.* (2004) provided a detailed description of this model. Note that a SCM test can also be viewed as a useful modeling check on the quality of the derived forcing data. In the SCM runs, the large-scale total advective tendencies of temperature (including the adiabatic expansion term) and moisture are specified from the four different forcing datasets derived from the analysis experiments Exp0, Exp1, Exp2, and Exp3, respectively. In all the runs, the model surface is defined as land. The surface temperature, pressure, broadband albedo, and sensible and latent heat fluxes are specified from the observations. To prevent serious drift of SCM simulations, a series of 30-hour forecast runs is initiated at 11Z every day. For each forecast, the temperature and moisture are initialized with the observations and the model clouds are set to zero at the beginning. A composite of 6 – 30 hour forecasts from the series of 30-hour runs is analyzed to reduce model spin-up problems and to give time for model clouds to develop. For convenience in the following discussions, we use SCMExp0, SCMExp1, SCMExp2, and SCMExp3 to represent the SCM run with the forcing data derived from the experiments Exp0, Exp1, Exp2, and Exp3, respectively.

Figure 11 shows the simulated temperature and moisture errors from the SCMExp0 run compared to observations. Results are very similar when the model is driven by the other three

forcing datasets (not shown). Model errors are typically less than 4 K and 1 g kg^{-1} for most of the period except during the strong frontal passage on 19 October, where the model shows a large cold bias in the upper troposphere and a large warm bias in the middle and lower troposphere. Note that this is a typical error pattern shown in most SCMs in simulating strong frontal cloud systems, including those observed in the middle latitudes [e.g., *Xie et al.* 2005]. A similar error pattern is also seen in the Goddard Institute for Space Studies (GISS) SCM [*Del Genio et al.*, 2005] with the forcing data from the control analysis (Exp0) (Audrey Wolf of GISS, personal communication). Note that the parameterizations of cloud condensations, cloud fraction, and cumulus convection used in the GISS model are significantly different from the NCAR model as described in *Xie et al.* [2005]. This could suggest potential errors in the analyzed large-scale forcing in addition to model deficiencies. It is known that subgrid-scale dynamical and thermodynamical processes have a large influence on frontal circulations. These subgrid-scale processes cannot be fully described in the large-scale forcing data that are derived from only limited sounding stations. As indicated by *Xie et al.* [2005], many of the SCM errors in simulating frontal systems could be traced to the lack of subgrid-scale dynamical structure in the applied forcing fields.

Figure 12 displays the SCM-simulated cloud fields from the SCM runs. In comparison with the observations (Figure 5a), it is encouraging to see that the model is able to generally capture well the various cloud types observed during M-PACE using all four forcing datasets (Figures 12a-d). For example, the model reproduces the multi-layer clouds on 6-7 October, the boundary layer clouds between 8 – 14 October, and the high frontal clouds on 18-19 October as shown in Figure 5a. However, the model largely underestimates the multilayered clouds and boundary layer clouds in the observed cloud layer when quantitatively compared to the observations. The model-produced boundary layer cloud bases are lower than the observed. This model error is also seen in the simulations of its parent GCM (CAM3) for this case (not shown), in which CAM3 was initialized with the NASA global analysis data [*Xie et al.* 2006b]. It is worth noting that the cloud base in the ARSCL products is determined by the ARM laser ceilometers and micropulse lidars, which are usually insensitive to ice precipitation (if the concentration of precipitation particles is not sufficiently large) or clutter and can provide quite accurate cloud base measurements [*Clothiaux et al.*, 2000]. The SCM also misses the mid- and low-level clouds below 615 hPa on 18 October, which could partly contribute to the warm bias

shown on Oct. 18-19 in Figure 11a due to the lack of cloud radiative cooling. Another interesting feature is that all the runs generate unrealistic high clouds on 7 October. This is most likely due to the quite strong upper level upward motion and cold advection shown in the forcing field (Figures 6a-b), which might not be realistic.

While the overall structure of the simulated Arctic clouds is very similar in these runs regardless of which forcing dataset is used, there are some slight differences among the simulations. One noteworthy feature is that the SCMExp3-predicted low-level clouds for the period 8-12 October are too low with the cloud bases almost reaching the surface. This problem is reduced in the other three runs, in which the predicted low-level cloud bases are between 965 and 915 hPa. This indicates that including the surface heat fluxes over the ocean part of the analysis domain helps lift the low-level model clouds from the surface, which is more realistic. It should be noted that this improvement is not a result of using the slightly different forcing datasets as shown in Figure 10, but is a result of using larger surface sensible and latent heat fluxes to specify the surface conditions in these SCM runs (SCMExp0-2) than in the SCMExp3 run, in which only the heat fluxes over land are used. Another notable feature is that SCMExp2 predicts slightly more clouds than the other three runs, consistent with the stronger upward motion in the Exp2 forcing data due to the larger surface precipitation constraint used in the analysis.

Figures 13a-d compare the SCMExp0-simulated surface precipitation (PREC), cloud liquid water path (LWP), TOA outgoing longwave radiative flux (OLR), and surface downward shortwave radiative flux with the observations. Results are very similar for the three other SCM runs (not shown). The temporal correlation between the runs SCMExp1, SCMExp2, SCMExp3 and the control run SCMExp0 is generally larger than 0.95 for these fields. In general, the model is able to capture the observed surface precipitation, such as the weak precipitation events in the early period of the experiment and the strong frontal precipitation on late 19 October. The model also performs a decent job on capturing the observed liquid water path for the period 8-14 October where boundary layer clouds appeared. It is noteworthy that almost all the model cloud water is in liquid phase and only a small amount of cloud water is in ice phase (the thin solid line in Figure 13b). In contrast, the observed clouds contained a significant amount of ice as indicated by the cloud radar, cloud micropulse lidar, and aircraft measurements [McFarquhar *et al.*, 2005]. It is seen that the model produces little ice even during the periods when the

multilayered clouds and the high frontal clouds are generated, which leads to a significant overestimation of the observed LWP. The model considerably overpredicts TOA outgoing longwave radiative flux and the downward surface shortwave radiation in the presence of boundary layer clouds, consistent with the underestimation of the low-level clouds. It is worth noting that these model errors revealed from the SCM tests are also seen in its parent GCM runs (not shown), suggesting potential model deficiencies in simulating the Arctic mixed-phase boundary clouds.

Table 2 lists the time-mean values of some selected cloud and radiation related fields averaged over the period from 17Z 5 October to 14Z 20 October, where the sequential 6 – 30 hours model forecasts are available. In the table, LWP is cloud liquid water path, IWP is cloud ice water path, OLR is TOA outgoing longwave radiative flux, FSNT is TOA net shortwave radiative flux, FSNS is surface net SW radiative flux, FLNS is surface net longwave radiative flux, PREC is surface precipitation, and TPW is total precipitable water. The observed precipitation used in deriving the forcing data from Exp2 is listed in parentheses. Note that results from the SCM driven with the forcing data derived from the ECMWF analyses are also shown in the table (the last column), which will be discussed in the next section.

One noteworthy feature in Table 2 is that the NCAR model shows very similar model bias in most of the fields regardless of which forcing dataset is used. For example, all the SCM runs (i.e., SCMExp0-3) dramatically overestimate the observed cloud liquid water path (LWP) and they all produce very little ice (IWP). For the radiation field, these runs slightly overestimate the observed TOA shortwave radiation (FSNT) by around $1.4\text{--}2.3\text{ Wm}^{-2}$ but largely overpredict the net surface SW radiation (FSNS) by up to 6.8 Wm^{-2} . The latter is associated with the underestimation of the boundary clouds. The underestimation of the observed low-level clouds also leads to an overprediction of OLR at TOA and an under-prediction of downward LW radiation at the surface. The latter results in a larger net surface longwave radiative cooling (FLNS) compared to observation. Note that the model-predicted surface upwelling longwave radiation is close to the observations because the model surface temperature is specified from the observations. It is interesting to see that SCMExp3 produces smaller errors in the surface downward LW radiation than other runs. This is due to the lower cloud base produced in the SCMExp3 run. All the runs reproduce well the observed surface precipitation (PREC). As expected, SCMExp2 produces larger precipitation than other runs because of the stronger

upward motion in the forcing data it used. SCMExp1 produces larger precipitation in comparison with the control case SCMExp0, presumably due to the higher temporal variability in the derived forcing fields as noted in Figure 10a. All the runs just slightly underestimate the observed column total precipitable water (TPW).

The above discussions indicate that the SCM driven with the forcing data derived in this study can reasonably generate the various cloud types in the observed Arctic cloud systems and the associated surface precipitation events during the M-PACE period. Several major model errors in simulating the Arctic cloud systems can be detected despite the uncertainties in the derived forcing data. This provides confidence in using the analyzed forcing data for more in-depth SCM and CRM study of the Arctic clouds.

It should be noted that these results are only from the NCAR SCAM3 model tests. Other SCMs might respond to the uncertainties in the forcing data differently. Also our focus here is to demonstrate how sensitive SCM simulations are to the uncertainties in the forcing data. A more in-depth analysis is needed to fully interpret model results and understand the causes of those model errors, which is the subject of a separate study.

6. Forcing data derived from the ECMWF analyses

It is always difficult to obtain comprehensive sounding data from a well-defined sounding array for the purpose of deriving the large-scale forcing fields, especially in the Arctic. Moreover, it is almost impossible to have such soundings for a period that is longer than a few months. However, a long-term continuous forcing dataset is necessary for SCM/CRM modelers to statistically evaluate their model performance. To develop such a long-term forcing dataset, NWP model analyses have to be used. Given the good quality of the ECMWF analyses as shown in Figure 2 and also in *Xie et al.* [2006a], we explore the possibility of using the ECMWF analyses to derive the large-scale forcing over the Arctic region in this section. As discussed by *Xie et al.* [2003] and *Morrison and Pinto* [2004], the forcing data directly obtained from the ECMWF model contain large errors. Similar problems are found in other NWP model-derived forcing data, such as in those generated from the NOAA rapid update cycle (RUC) model forecast analysis data [*Xie et al.*, 2004]. Several approaches were proposed to reduce errors in the NWP model-derived forcing data by using available observations to constrain the NWP data [e.g., *Xie et al.*, 2004; *Morrison and Pinto*, 2004]. In this study, we use the method described in

Xie et al. [2004] to derive the large-scale forcing data from the ECMWF analyses for the M-PACE period. In this approach, the M-PACE surface and TOA fluxes are used as the constraints to adjust the ECMWF analysis data so that they are forced to balance the observed column budgets of mass, heat, moisture, and momentum by using the variational analysis method. For convenience in the following discussions, we use “ECMWF forcing” to refer to the forcing derived from the ECMWF analyses and “analyzed forcing” to represent the forcing derived from the M-PACE sounding data.

Figures 14a-b shows the derived large-scale omega field from the ECMWF analyses and the difference from that generated in the control analysis (Exp0). It is encouraging to see that the ECMWF-produced omega shows a very similar distribution compared to the analyzed (Figure 6a). However, the vertical motion in the ECMWF model is weaker and smoother than that in the analysis, reflecting more homogenous horizontal wind fields in the model than those in the sounding data. The difference between these two forcing datasets (Figure 14b) is much larger than that due to the uncertainties in the sounding measurements and surface constraints as shown in Figures 10d-f. This indicates that the derived forcing fields are sensitive to the small differences between the ECMWF model analysis and the observations in these state variables at individual stations, although the magnitude of the RMS errors in the ECMWF analysis data is small as shown in Figure 2. To correctly capture the magnitude and temporal and spatial variability of the large-scale forcing fields, measurements from a well-defined sounding array are necessary.

To examine how SCMs respond to the ECMWF forcing, we ran the SCAM3 with the ECMWF forcing in the same way as we did for the SCM tests with the analyzed forcing datasets in Section 5. For convenience in this discussion, we use SCMEC to represent this SCM run. Simulation results show that SCMEC produces very similar and comparable temperature and moisture errors when compared to the SCM forced with the analyzed forcings (not shown). However, some noticeable differences are seen in the simulated cloud field. Figure 15 shows the clouds simulated by SCMEC. When compared to Figure 12, it is seen that although the overall structure of the model-produced clouds is similar between the SCMEC run and the SCM runs with the analyzed forcing, differences are noticed. For example, SCMEC produces less mid-level cloud for the multilayered cloud system on 6-7 October and it also misses the deep upper-level cloud on 18 October in comparison with the SCM runs with the analyzed forcing datasets.

It is interesting to see that the spurious upper-level cloud shown on 7 October in Figure 12 is not present in Figure 15. This is because the ECMWF forcing does not have the upward motion on 7 October in the upper troposphere as shown in the analyzed forcing field (Figure 6a).

The time-averaged values of the selected cloud and radiation related fields from SCMEC are listed in the last column in Table 2. In general, the model errors shown in the runs with the analyzed forcing datasets are also seen in SCMEC. For example, the model with the ECMWF forcing also produces too much cloud liquid water. It overestimates OLR and net SW at TOA and overestimates net LW cooling and SW heating at the surface. The surface precipitation and total precipitable water are well reproduced. In general, SCMEC shows larger errors than the runs driven by the analyzed forcing. Results from SCMEC are less correlated to those from SCMExp0 compared to those runs discussed in Section 5. The temporal correlation coefficient for some fields, such as OLR and FLNS, is just around 0.5. This indicates that the SCM driven with the ECMWF forcing may statistically detect the major model errors as revealed by the SCM using the analyzed forcing, but noticeable differences exist in the time evolution of these fields simulated by these two types of forcing datasets. With further improvements in both quality and data density of surface measurements over the Arctic region in the future, it may be possible for us to derive a long-term multi-year forcing data from ECMWF analyses over the NSA region.

7. Summary and discussions

Developing large-scale SCM/CRM forcing data from observations in the high latitudes has been impossible in the past, owing to the lack of a suitable sounding array. The situation is improving with the ARM Mixed-Phase Arctic Cloud Experiment that was recently conducted over the North Slope of Alaska in October 2004. In this field campaign, a sounding array of four stations launched sounding balloons four times per day to measure the time evolution of the Arctic atmosphere and allow for calculation of the large-scale advection of temperature and moisture. In this study, we have used the objective analysis method of *Zhang and Lin* [1997] to derive the highly desired forcing data in the Arctic region for the first time based on the M-PACE observations. The technical details of the objective analysis and several important technical and scientific issues related to the analysis have been discussed in this paper.

It has been shown that the analyzed large-scale vertical velocity and advective tendencies of temperature and moisture describe the dynamic and thermodynamic structure of the observed

Arctic cloud systems reasonably well. For the observed multilayered clouds and boundary layer clouds, the analyzed data typically show strong downward motion above cloud top and relatively weak upward motion at low levels. The downward motion is much stronger and extends to much lower levels for the period where only low-level clouds were observed. Generally there is warm temperature advection above cloud top and cold advection at low levels associated with the downward and upward motions, respectively. The analyzed moisture forcing indicates quite strong moisture convergence at middle levels prior to the formation of multilayered clouds and it generally shows moisture divergence for most of the period where boundary layer clouds occurred, suggesting that the observed boundary layer clouds formed over the nearby oceans and advected into the ARM NSA site.

It is noted that there are only three surface observation stations at the NSA site. The lack of dense surface observations could affect the accuracy of the surface domain-averaged quantities. Using the ECMWF 0.5 x 0.5 model output data, we have shown that this could introduce an uncertainty of more than 20% in the domain-averaged surface precipitation and sensible and latent heat fluxes. Increasing the density of surface observation networks is important to improve the domain-average quantities and thereby improving the analyzed large-scale forcing fields.

To estimate the accuracy of the analyzed forcing fields, we have examined the sensitivity of the forcing data to uncertainties in the upper-air data, surface precipitation, and sensible and latent heat fluxes. It has been shown that the analyzed forcing data derived from these sensitivity tests exhibit very similar dynamic and thermodynamic structures as shown in the control analysis. The largest sensitivity of the analyzed forcing is to uncertainties in the surface precipitation constraint, consistent with *Zhang et al.* [2001]. Given the large uncertainty in current surface precipitation measurements at the NSA site and its importance in the analyzed forcing fields, significant efforts need to be given to improve the quality and data density of surface precipitation measurements in the future.

The NCAR CAM3 single column model has been used to examine how the uncertainties in the forcing data affect model simulations. It has been shown that the SCM driven with the analyzed forcing data is able to capture qualitatively the bulk features of the Arctic cloud systems observed during M-PACE. Similar results are produced in these SCM tests regardless of which forcing data are used, indicating that major model biases can be detected using the

analyzed forcing data developed in this study. It is worth noting that most model errors revealed in the SCM tests are also seen in its parent GCM simulations for the M-PACE case, as found in a separate study [Xie *et al.* 2006b]. These encouraging results provide confidence in using the analyzed M-PACE forcing data for a more in-depth SCM/CRM study of the Arctic clouds.

To explore the possibility of using NWP data to derive the large-scale forcing over the Arctic region, we have used the ECMWF analyses to replace the M-PACE soundings in the data analysis. The ECMWF analyses are adjusted to balance the M-PACE observed column-integrated budgets of mass, heat, moisture, and momentum through the variational analysis approach. It has been shown that the forcing data derived from the ECMWF analyses display similar temporal and vertical structures compared to those derived from the M-PACE soundings but the ECMWF forcing fields are generally weaker and smoother. The NCAR SCM driven by the ECMWF forcing is able to produce similar simulations in most atmospheric fields as those obtained in the SCM driven with the analyzed forcing but with larger errors. Major model errors related to clouds can be detected in a statistical way using the ECMWF forcing, such as the substantial overestimation of the observed cloud liquid water. This indicates that it may be possible for us to develop a long-term continuous forcing dataset from ECMWF analyses in the high latitudes for statistical study with further improvements of surface measurements in those regions in the future.

It has been shown that the data availability in M-PACE and inevitable errors in the data measurements largely limit the accuracy of current analyzed products. Improvements in both data quality and density of field measurements in the future are critical to improve the accuracy of the derived large-scale forcing data. Developing an ensemble of forcing datasets based on potential uncertainties in upper-air data and column constraints might help address the uncertainty in the analyzed forcing data. In addition, it also allows modelers to run their SCMs using an ensemble single column modeling approach as suggested in Hume and Jakob [2005], in order to reduce the sensitivity of SCMs to uncertainties in the forcing data.

It should be noted that this study has only tested the forcing datasets in one SCM. The datasets need to be further evaluated using different SCMs and CRMs since different models may respond the uncertainties in the forcing data in different ways. This is a subject of future work. The forcing data developed from the control run in this study are being used in the ARM

Cloud Parameterization and Modeling Working Group for a modeling study of the Arctic mixed-phase boundary layer clouds during M-PACE. The data can be obtained from the website: <http://science.arm.gov/wg/cpm/scm/scmic5/index.html>. This paper has attempted to address several important issues related to the analyzed data developed in this study and it should be useful for modelers to use the data and interpret their model results. It also provides information that could be used to guide future field experiments in the high latitudes.

Acknowledgments. The authors would like to thank the three anonymous reviewers for their valuable comments that helped to clarify and improve the paper. We gratefully thank Drs. J. Verlinde, J. Mather, C. Bahrmann, C. Long, P. Heck, P. Minnis, M. Miller, K. Johnson, and J. Pinto for making the M-PACE data available for our use. We thank Dr. Anton Beljaars of ECMWF and Dr. Eric Rogers of NCEP for generously providing us the ECMWF model and NCEP ETA model forecast analysis data. Special thanks go to Dr. Chris Fairall for providing us with the code for calculating the surface sensible and latent fluxes, to Karen Johnson for helping us with the use of the ARSCL cloud data. Feedbacks from Drs. H. Morrison, J. Pinto, A. Del Genio, A. Wolf, I. Sednev, and S. Menon have helped us to improve the analysis data. The observational data were obtained from the ARM program sponsored by the U. S. Department of Energy, Office of Science, Office of Biological and Environmental Research, Environmental Sciences Division. This research was performed under the auspices of the U. S. Department of Energy by the University of California, Lawrence Livermore National Laboratory, under contract W-7405-Eng-48. Work at SUNY Stony Brook was supported by the DOE ARM program under grant EFG0298ER62570.

References

- Barnes, S. L. (1964), A technique for maximizing details in numerical map analysis, *J. Appl. Meteor.*, 3, 396-409.
- [Collins, W. D.](#), P. J. Rasch, B. A. Boville, J. J. Hack, J. R. McCaa, D. L. Williamson, J. T. Kiehl, B. Briegleb, C. Bitz, S.-J. Lin, M. Zhang, and Y. Dai (2004), [Description of the NCAR Community Atmosphere Model \(CAM3\)](#), Technical Report NCAR/TN-464+STR, NCAR, Colorado, 226 pp.
- Cressman, G. P., (1959), An operational objective analysis scheme, *Mon. Wea. Rev.*, 87, 367-374.
- Clothiaux, E. E., T. P. Ackerman, G. G. Mace, K. P. Moran, R. T. Marchand, M. Miller, and B. E. Martner (2000), Objective determination of cloud heights and radar reflectivities using a combination of active remote sensors at the ARM CART sites, *J. Appl. Meteor.*, 39, 645-665.
- Del Genio, A.D., W. Kovari, M.-S. Yao, and J. Jonas, Cumulus microphysics and climate sensitivity (2005), *J. Climate*, 13, 2376-2387.
- ECMWF (2004), The ECMWF operational analysis and forecasting system: The full evolution, Reading, United Kingdom. (Available from http://www.ecmwf.int/products/data/operational_system/evolution/evolution_2004.html#28 September2004)
- Fairall C. W., E. F. Bradley, D. P. Rogers, J. B. Edson, and G. S. Young (1996), Bulk parameterization of air-sea fluxes for Tropical Ocean-Global Atmosphere Coupled-Ocean Atmosphere Response Experiment, *J. Geophys. Res.*, 101, 3747-3764.
- Harrington J. and J. Verlinde (2004), Mixed-phase Arctic Clouds Experiment (M-PACE). The ARM Scientific Overview Document, U. S. Dep. of Energy, Washington, D. C. 1998.
- Hume and Jacob (2005), Ensemble single column modeling (ESCM) in the tropical western Pacific: Forcing data sets and uncertainty analysis, *J. Geophys. Res.*, 110, D13109, doi: 10.1029/2004JD005704.
- Jiang, H., W. R. Cotton, J. O. Pinto, J. A. Curry, and M. J. Weissbluth (2000), Cloud resolving simulations of mixed-phase Arctic stratus observed during BASE: Sensitivity to

- concentration of ice crystals and large-scale heat and moisture advection, *J. Atmos. Sci.*, 57, 2105-2117.
- Lesht, B. M. (2005), Balloon-Borne Sounding System (BBSS) Handbook. ARM Technical Report 029, 29 pp. Washington D. C. (Available from http://www.arm.gov/publications/tech_reports/handbooks/sonde_handbook.pdf)
- McFarquhar, G., G. Zhang, J. Verlinde, M. Poellot, A. Heymsfield, and G. Kok (2005), Assessing current parameterization of mixed-phase clouds using in situ profiles measured during the Mixed Phase Cloud Experiment, *Fifteenth ARM Science Team Meeting Proceedings*, Daytona Beach, Florida, March 14-18, 2005.
- Minnis, P., W. L. Smith, D. F. Young, L. Nguyen, A. Rapp, P. W. Heck, S. Sun-Mack, Q. Z. Trepte, and Y. Chen (2001), A near-real time method for deriving cloud and radiation properties from satellites for weather and climate studies, *Proc. AMS 11th Conf. Satellite Meteorology and Oceanography*, Madison, WI, October 15-18, 477-480.
- Morrison, H., and J. O. Pinto (2004), A new approach for obtaining advection profiles: Application to the SHEBA column, *Mon. Weather Rev.*, 132, 687-702.
- Pinto, J. O., J. A. Curry, and A. H. Lynch (1999), Modelling clouds and radiation for the November 1997 period of SHEBA using a column climate model, *J. Geophys. Res.*, 104, 6661-6678.
- Randall, D. A., K-M. Xu, R. J. C. Somerville and S. Iacobellis (1996), Single-column models and cloud ensemble models as links between observations and climate models, *J. Climate*, 9, 1683-1697.
- Rogers, E., T. Black, B. Ferrier, Y. Lin, D. Parrish, and G. DiMego (2001), Changes to the NCEP Meso Eta analysis and forecast system: Increase in resolution, new cloud microphysics, modified precipitation assimilation, modified 3DVAR analysis, NWS Technical Procedures Bulletin 488, NOAA/NWS, Washington, D. C.
- Verlinde, J. and Coauthors (2005), Overview of the Mixed-Phase Arctic Cloud Experiment (M-PACE), paper presented at 85th AMS Annual Conference Proceedings, San Diego, California.
- Xie, S., S. A. Klein, J. J. Yio, A. C. M. Beljaars, C. N. Long, and M. Zhang (2006a), An assessment of ECMWF analyses and model forecasts over the North Slope of Alaska using

- observations from the ARM Mixed-Phase Arctic Cloud Experiment, *J. Geophys. Res.*, *111*, D05107, doi:10.1029/2005JD006509.
- Xie, S., S. A. Klein, J. Boyle, M. Forino, J. Hnilo, T. Phillips, G. Potter, and A. Beljaars (2006b), Validation of Global Weather Forecast and Climate Models Over the North Slope of Alaska. *Sixteenth ARM Science Team Meeting Proceedings*, Albuquerque, New Mexico, March 27-31, 2006.
- Xie, S. C., M. Zhang, M. Branson, R. T. Cederwall, A. D. Del Genio, Z. A. Eitzen, S. J. Ghan, S. F. Iacobellis, K. L. Johnson, M. Khairoutdinov, S. A. Klein, S. K. Krueger, W. Lin, U. Lohmann, M. A. Miller, D. A. Randall, R. C. J. Somerville, Y. C. Sud, G. K. Walker, A. Wolf, X. Wu, K. Xu, J. Yio, G. Zhang, and J. Zhang (2005), Simulations of midlatitude frontal clouds by single-column and cloud-resolving models during the Atmospheric Radiation Measurement March 2000 cloud intensive operational period, *J. Geophys. Res.*, *110* D15S03, doi:10.1029/2004JD005119.
- Xie, S. C., R. T. Cederwall, and M. Zhang (2004), Developing long-term single-column model/cloud system-resolving model forcing data using numerical weather prediction products constrained by surface and top of the atmosphere observations, *J. Geophys. Res.*, *109* D001104, doi:10.1029/2003JD004045.
- Xie, S. C., R. T. Cederwall, M. Zhang, and J. Yio (2003), Comparison of SCM and CSRM forcing data derived from the ECMWF model and from objective analysis at the ARM SGP, *J. Geophys. Res.*, *108* (D16), 4499, doi:10.1029/2003JD003541.
- Zhang, M. H., and J. L. Lin (1997), Constrained variational analysis of sounding data bases on column-integrated budgets of mass, heat, moisture, and momentum: Approach and application to ARM measurements, *J. Atmos. Sci.*, *54*, 1503-1524.
- Zhang, M. H., J. L. Lin, R. T. Cederwall, J. J. Yio, and S. C. Xie (2001), Objective analysis of ARM IOP Data: Method and sensitivity, *Mon. Weather Rev.*, *129*, 295-311.

Figure Captions

- Figure 1.** Locations of the ARM M-PACE sounding network and the analysis grid points. The sounding stations are represented by (*), the six analysis grid points are displayed by (•), and the ECMWF model output grid points are “+” with latitude and longitude lines indicated. The thin solid line represents the coastline.
- Figure 2.** The root-mean square errors of the ECMWF analysis (solid line) and the ETA analysis (dashed line) from the M-PACE observations at Barrow: (a) horizontal U wind component (m s^{-1}), (b) horizontal V wind component (m s^{-1}), (c) temperature (K), and (d) relative humidity (%).
- Figure 3.** The time series of (a) surface precipitation (mm day^{-1}), (b) surface net radiation (W m^{-2}), (c) sensible heat flux (W m^{-2}), and (d) latent heat flux (W m^{-2}) from the ECMWF gridded data during M-PACE. The solid line represents an average over all the land grid points within the analysis domain while the dashed line represents an average only over the single land grid points that are close to Barrow, Atqasuk, and Oliktok Point, respectively. The values shown behind the legends are the mean values averaged over the entire period.
- Figure 4.** Time-pressure cross sections of analyzed large-scale state fields: (a) horizontal U wind component (m s^{-1}), (b) horizontal V wind component (m s^{-1}), (c) temperature (c), and (d) water vapor mixing ratio (g kg^{-1}). In (a) and (b) the contour interval is 5 and contours less than 0 are drawn with dashed line. In (c) the contour interval is 5 and in (d) the contour intervals are 0.1, 0.3, 0.5, 1, 1.5, 2, 2.5, and 3.
- Figure 5.** (a) The time-pressure cross sections of the ARM ARSCL clouds (%) at Barrow during M-PACE (b) the domain-averaged surface precipitation (mm day^{-1}). In (b) the solid line represents the precipitation used in the control case Exp0 and the dashed line denotes the precipitation used in the sensitivity test Exp2. These experiments are described in Table 1.
- Figure 6.** Time-pressure cross sections of analyzed large-scale forcing fields: (a) vertical velocity (hPa hr^{-1}), (b) total advective tendency of temperature (K day^{-1}), and (c) total advective tendency of water vapor mixing ratio ($\text{g kg}^{-1} \text{day}^{-1}$).

Figure 7. Time series of the components in the dry static energy budget: (a) heat storage, (b) horizontal heat transport, (c) latent heat associated with precipitation, (d) sensible heat, and (e) column radiation. The units are W m^{-2} .

Figure 8. Time series of the components in the moisture budget: (a) moisture storage, (b) horizontal moisture transport, (c) surface precipitation, and (d) surface evaporation. The units are mm day^{-1} .

Figure 9. Time series of the domain-averaged (a) sensible heat flux (W m^{-2}) and (b) latent heat flux (W m^{-2}) during M-PACE. In the figure, solid lines represent the fluxes used in the control case Exp0 and dotted lines denote the fluxes used in the sensitivity test Exp3.

Figure 10. Time-pressure cross sections of analyzed vertical velocity fields from the sensitivity tests Exp1, Exp2, and Exp3 and their difference from the control case Exp0. The unit is hPa hr^{-1} .

Figure 11. The NCAR SCM-simulated temperature and moisture errors compared to the M-PACE observations. (a): temperature errors (K). (b): moisture errors (g kg^{-1}).

Figure 12. Time-pressure distributions of the NCAR SCM-simulated clouds and their difference from the ARM ARSCL clouds. The unit is %. (a) - (d) show the clouds produced by the SCMExp0, SCMExp1, SCMExp2, and SCMExp3, respectively.

Figure 13. Comparison of the NCAR SCM-produced (a) surface precipitation (mm day^{-1}), (b) cloud liquid water path (g m^{-2}), (c) TOA outgoing longwave radiation (W m^{-2}), and (d) surface downward shortwave radiation (W m^{-2}), with the M-PACE observations. The forcing data are from the control analysis Exp0. For comparison, the model-produced ice water path (g m^{-2}) is also shown in (b) by the thin solid line.

Figure 14. Same as Figure 10 except for the omega field derived from the ECMWF analyses.

Figure 15. Same as Figure 12 except for the results using the forcing data derived from the ECMWF analyses.

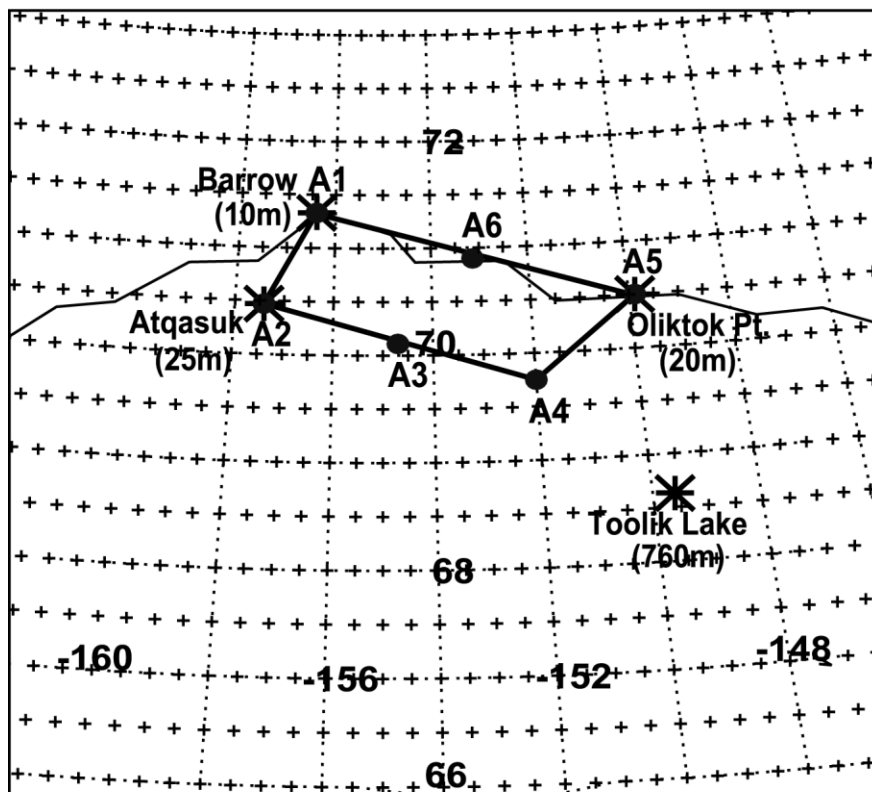
Table 1. Description of the sensitivity tests conducted in this study

Exp0	Control case
Exp1	Same as Exp0 except the upper-air data are randomly perturbed.
Exp2	Same as Exp0 except for using equal weights when merging the ARM and NWS precipitation. This results in a consistent increase of surface precipitation for each precipitation event because the ARM-observed precipitation is significantly larger than the NWS observed.
Exp3	Same as Exp0 except for using surface sensible and latent heat fluxes over land only. This results in a significant decrease of the fluxes for the period 5-13 October.

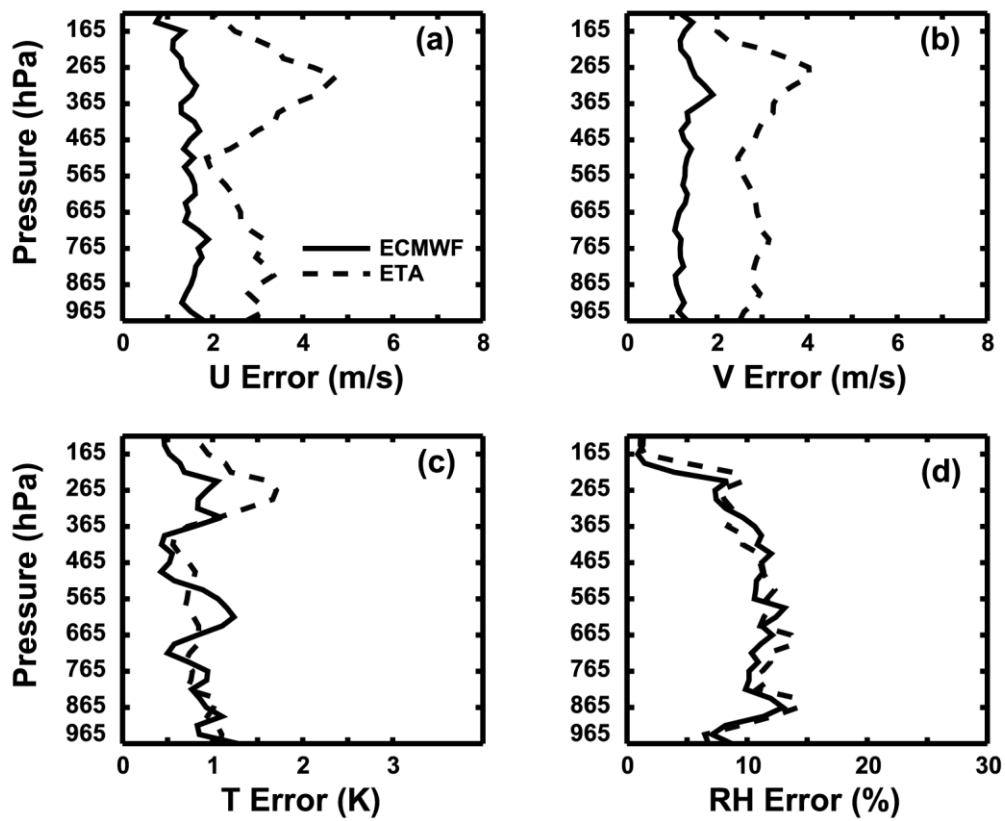
Table 2. Comparison of SCM simulations to M-PACE observations for selected cloud and radiation related fields. Values in the table are an average over the period from 17Z 5 October to 14Z 20 October. See the text for variable definitions.

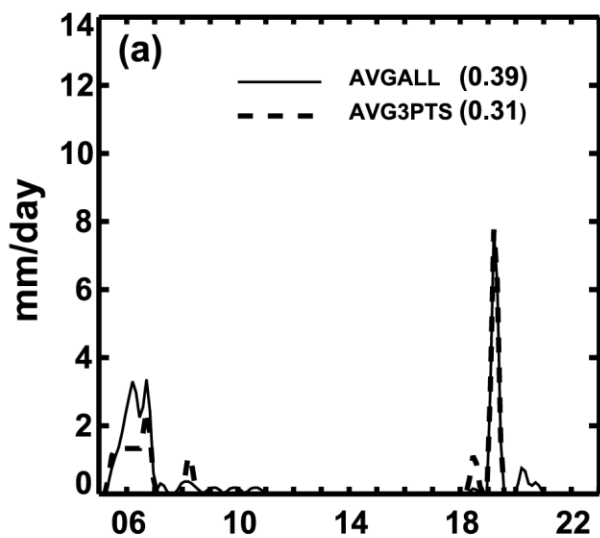
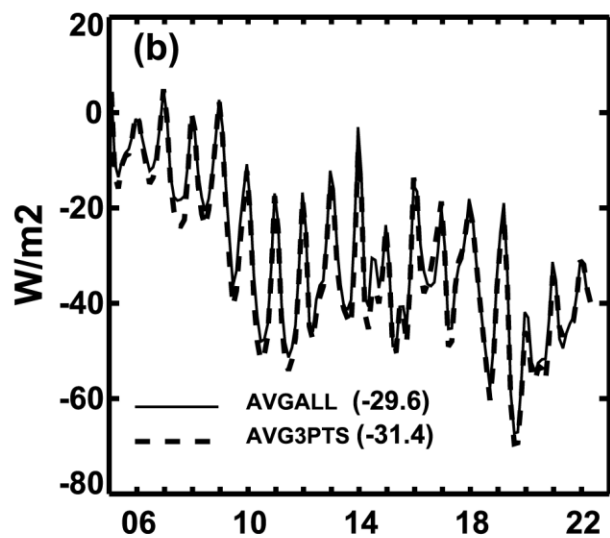
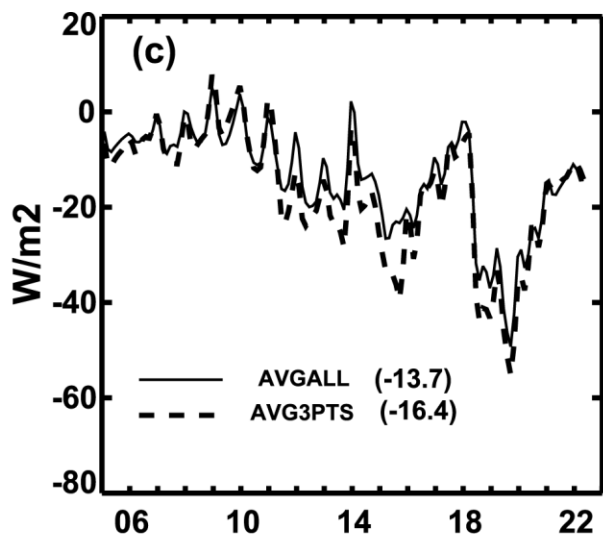
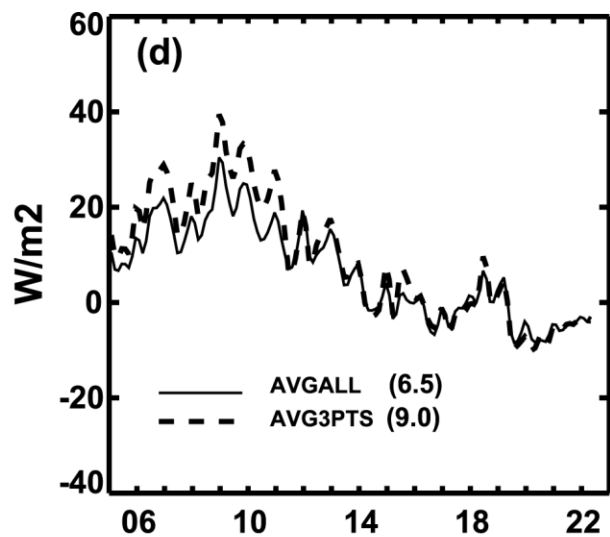
	OBS	SCMExp0	SCMExp1	SCMExp2	SCMExp3	SCMEC
LWP (g m^{-2})	72.0	141.1	145.1	168.4	160.3	148.5
IWP (g m^{-2})	N/A	13.4	14.0	18.2	15.1	10.65
OLR (W m^{-2})	204.2	212.9	212.4	210.2	211.7	217.2
FSNT (W m^{-2})	25.29	27.56	27.0	26.84	26.73	28.1
FSNS (W m^{-2})	3.78	10.6	10.0	9.88	9.68	10.5
FLNS (W m^{-2})	-18.3	-31.4	-30.6	-28.3	-22.3	-31.3
PREC (mm d^{-1})	0.76 (1.19)	0.75	0.79	(1.05)	0.77	0.69
TPW	7.67	7.35	7.36	7.52	7.34	7.17

Analysis Domain



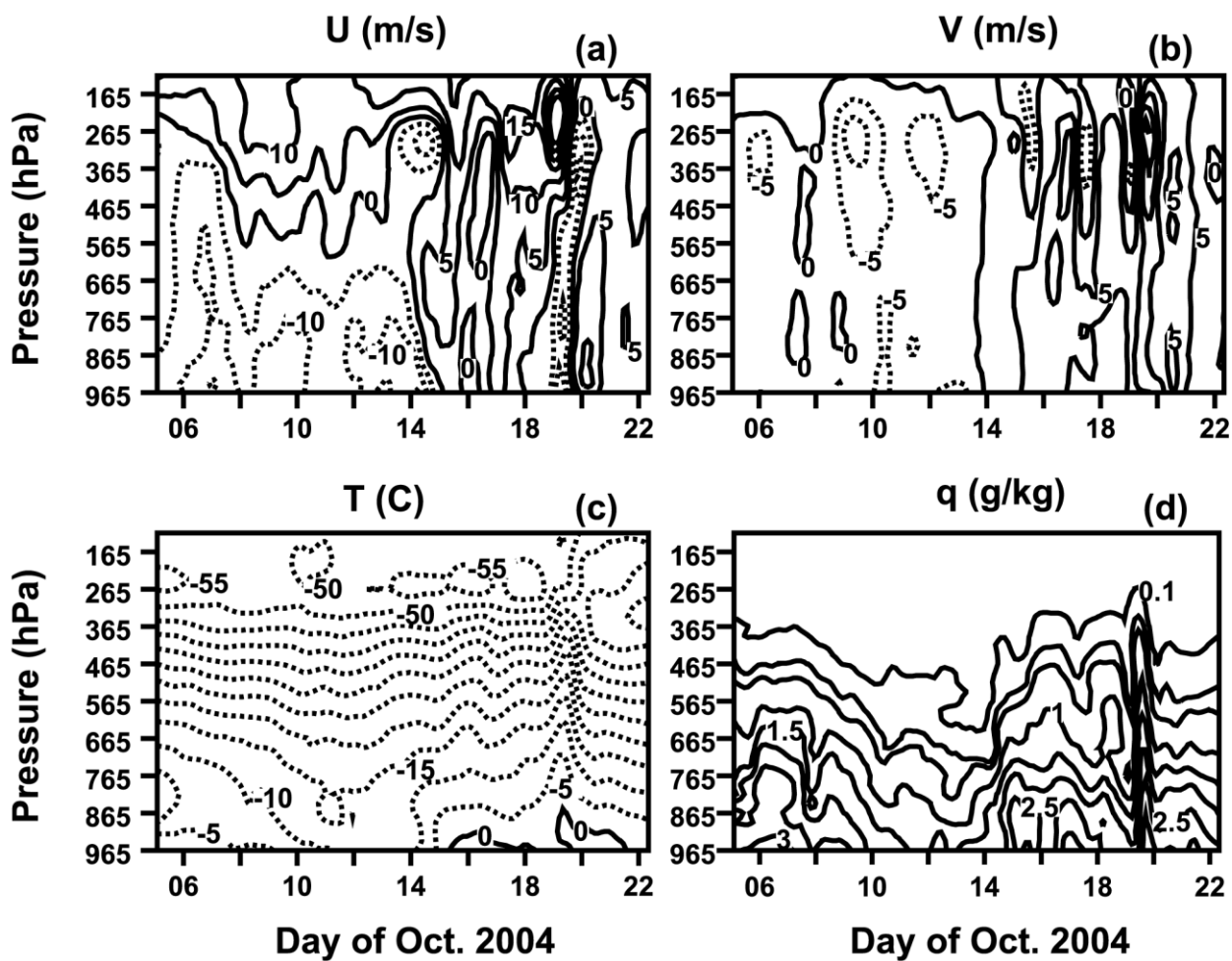
RMS Errors

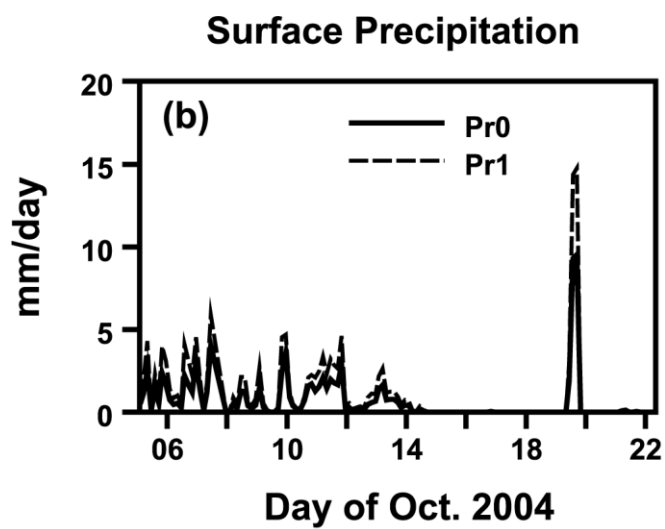
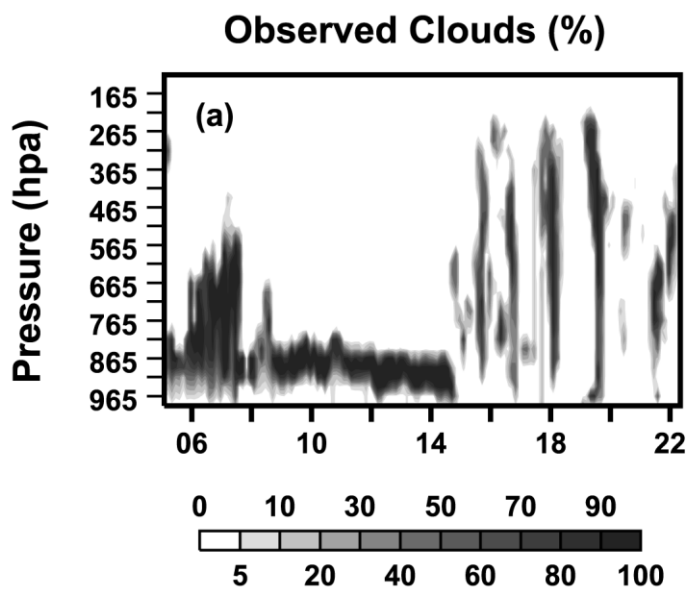


Surface Precipitation**Surface Radiation****Sensible Heat Flux****Latent Heat Flux**

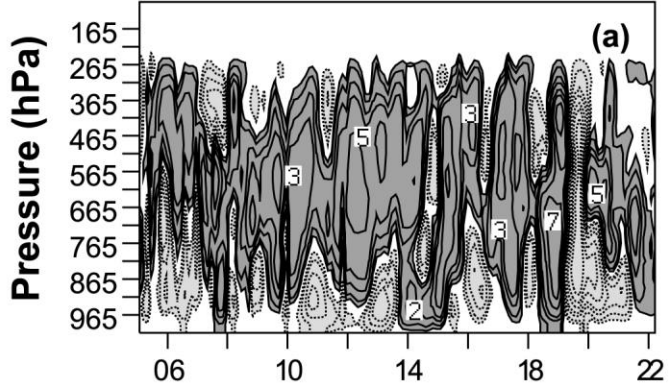
Day of Oct. 2004

Day of Oct. 2004

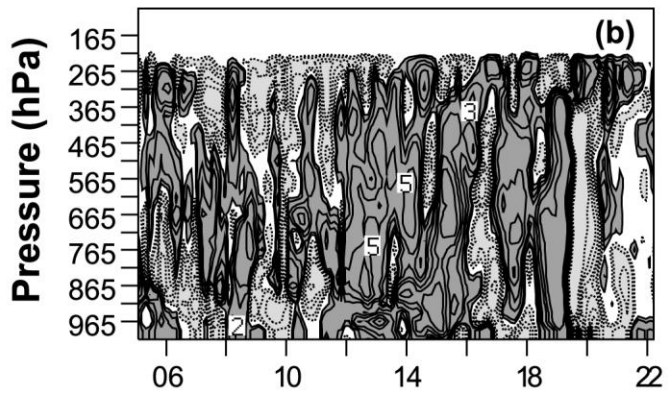




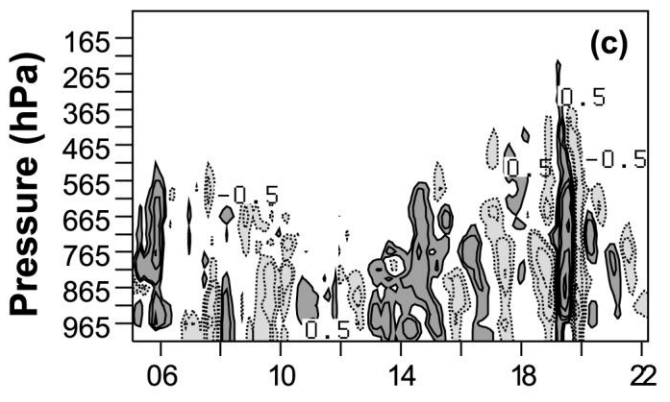
ARM Omega (hPa/hr)



Total Adv. of T (K/day)

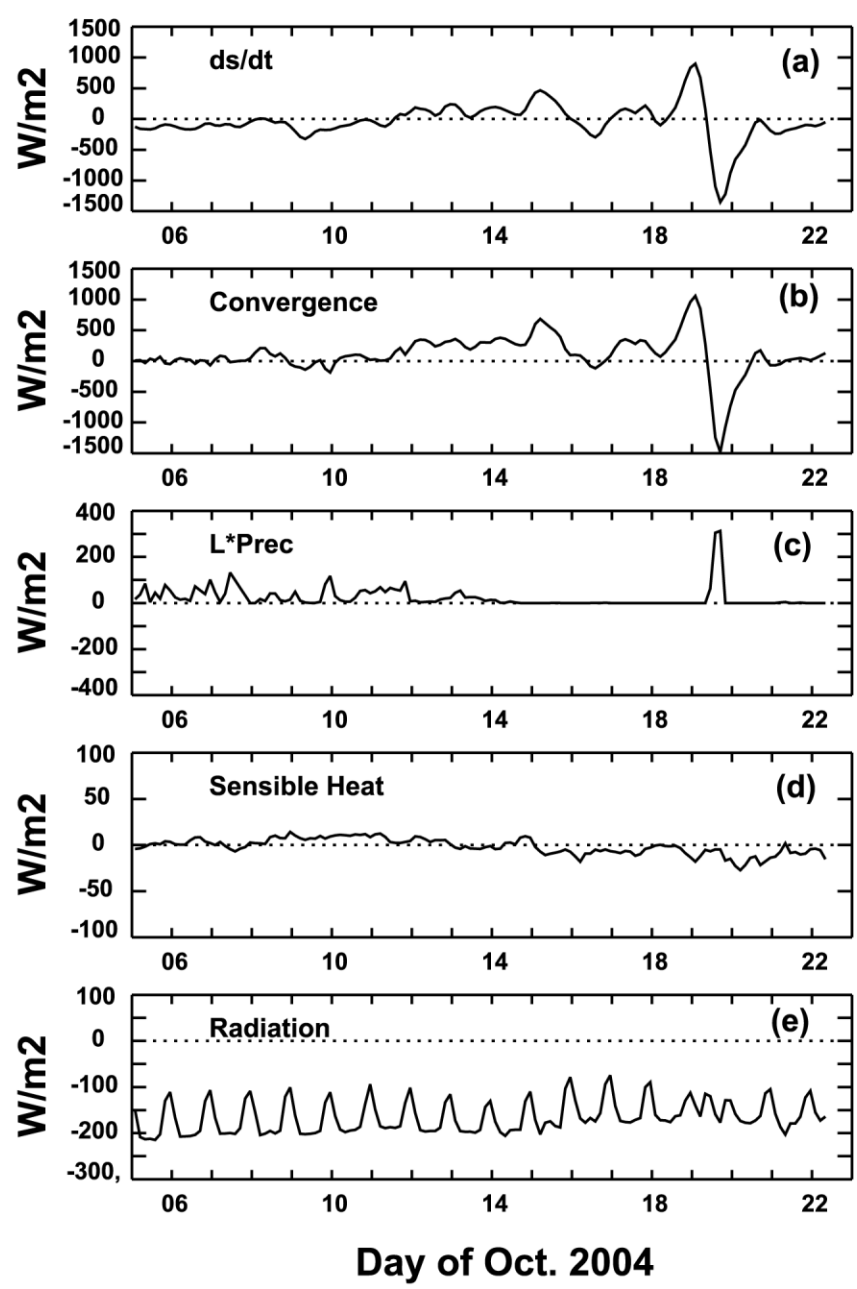


Total Adv. of q (g/kg/day)

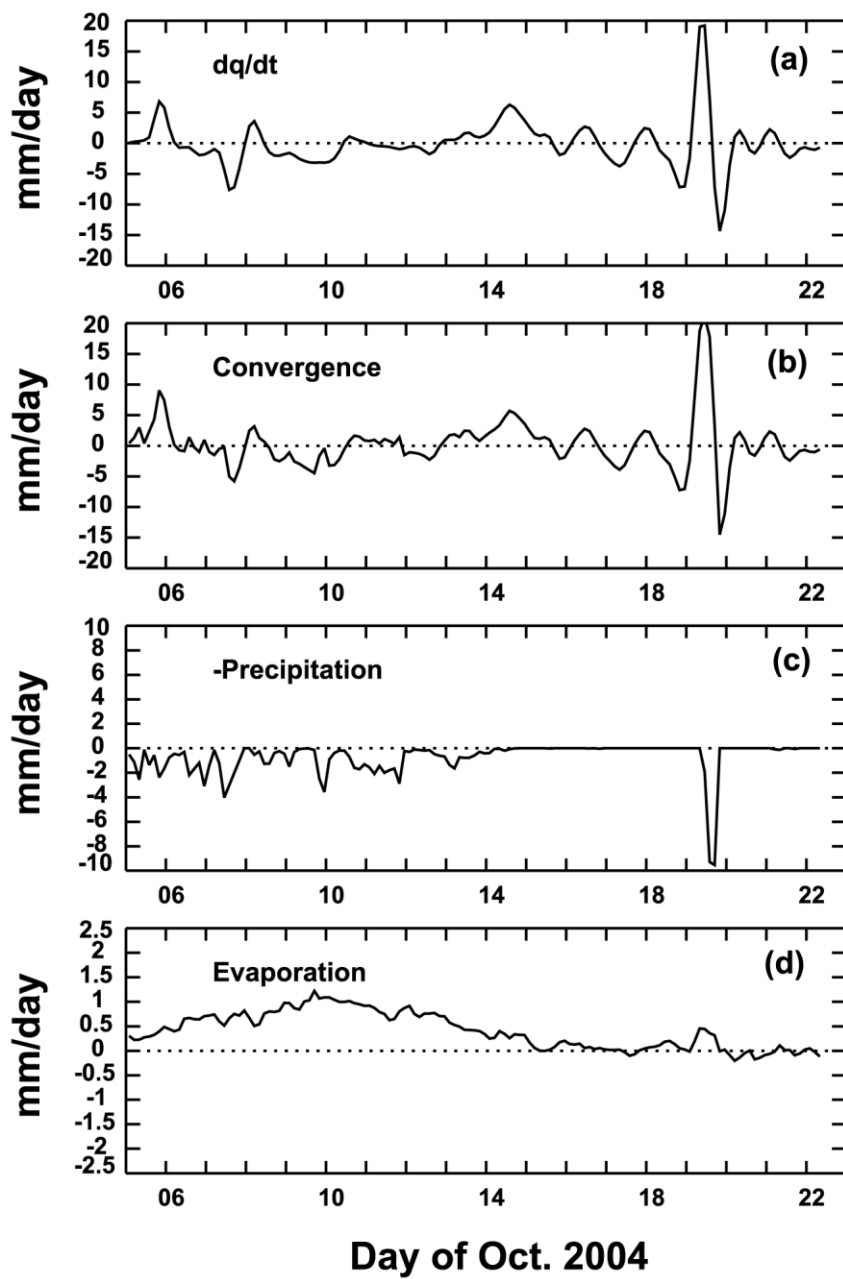


Day of Oct. 2004

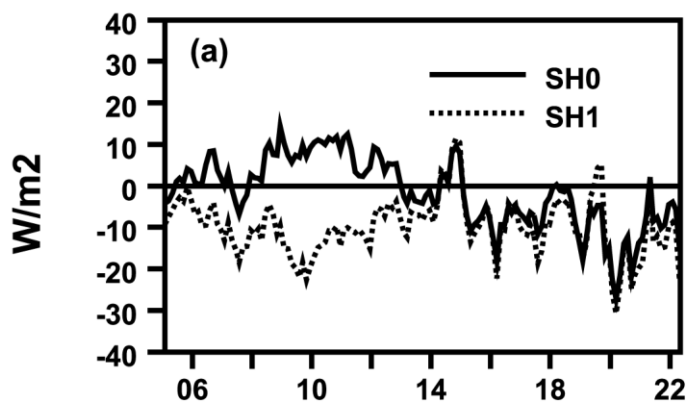
Dry Static Energy Budget Terms



Moisture Budget Terms



Sensible Heat Flux



Latent Heat Flux

